Short communication

High capacitance of surface-modified 2D titanium carbide in acidic electrolyte

Yohan Dall'Agnese [a,b,c], Maria R. Lukatskaya [c], Kevin M. Cook [c], Pierre-Louis Taberna [a,b], Yury Gogotsi [c], Patrice Simon [a,b,*]

[a] Université Paul Sabatier, CIRIMAT UMR CNRS 5085, 118 route de Narbonne, 31062 Toulouse, France
[b] Réseau sur le Stockage Electrochimique de l'Energie (RS2E), FR CNRS 3459, France
[c] Department of Materials Science and Engineering and A. J. Drexel Nanomaterials Institute, Drexel University, Philadelphia, PA 19104, USA

ARTICLE INFO

ABSTRACT

The electrochemical behavior of Ti_3C_2, a two-dimensional titanium carbide from the MXene family, in H_2SO_4 electrolyte is reported. To demonstrate the effect of surface chemistry on capacitive performance, Ti_3C_2 was modified by delamination or intercalation treatments. Electrochemical testing revealed an increase in capacitance, which was attributed to oxygen-containing functional groups. An extraordinary high intercalation capacitance of 415 F·cm^{-3} at 5 A·g^{-1} was obtained from electrodes with a specific surface area of just 98 m^2·g^{-1}. Values up to 520 F·cm^{-3} were recorded for delaminated MXene films at 2 mV·s^{-1}. This study highlights that the behavior of materials from the large family of two-dimensional MXene can be tuned by suitable modification of their surface chemistry.

1. Introduction

The development of suitable energy solutions to satisfy increasing energy demands is one of the key technological challenges our society is facing [1]. The main advantage of electrochemical capacitors (ECs) is that they can deliver high power densities (up to 20 kW kg^{-1}), however they suffer from a lower energy densities compared to batteries [2].

There are two types of ECs which differ by the charge storage mechanism realized in them: 1) electrical double layer capacitors, EDLCs, where charge is stored by electrosorption of ions at the electrode–electrolyte interface, and 2) pseudocapacitors, where charge is stored via fast surface redox reactions [3]. In case of EDLCs, capacitance is proportional to the materials' specific surface area, SSA. Therefore carbon-based materials are used since they exhibit high SSAs from 1000 to 2000 m^2·g^{-1}, giving capacitances up to 50–80 F·cm^{-3} and 150–200 F·g^{-1} [4]. The best known pseudocapacitive materials are MnO_2, RuO_2 and Nb_2O_5, since they provide multiple oxidation states during charge/discharge cycles and store the energy via reversible surface redox reactions [5–8]. Enhancement of the energy density can be achieved with hybrid materials, such as transition metal oxide particles inserted into porous carbon or chemically modified carbon with oxygen- or nitrogen-containing functional groups [4,9–15].

Our strategy is to develop new electrodes for aqueous supercapacitors from a new family of 2D materials called MXenes that have recently demonstrated promising results as electrodes for energy storage applications [16–25]. These so-named MXenes are synthesized by selectively etching out the A layers from MAX phases, a class of conductive ternary carbides and nitrides composed of an early transition metal, M, an element from group 13 or 14, denoted A, and carbon and/or nitrogen, X, with the general formula $M_{n+1}AX_n$ [26,27]. This synthesis yields electrically conductive MXene layers with −F and −OH/═O surface termination that can be abbreviated as T_x to give a general formula of $M_{n+1}X_nT_x$. $Ti_3C_2T_x$ has been investigated as electrode for lithium ion batteries and supercapacitors [17–20]. Moreover, the intercalation of a wide range of cations between $Ti_3C_2T_x$ layers, such as Li$^+$, Na$^+$, K$^+$, NH$_4^+$, Mg^{2+} and Al^{3+} has been demonstrated [19,20]. So far, the best electrochemical results were obtained for Ti_3C_2 "paper" electrodes prepared by filtration of the delaminated MXene few-layer flake solution, giving a capacity of 410 mAh·g^{-1} at 1C rate for Li-ion batteries and a high volumetric capacitance of up to 350 F·cm^{-3} for supercapacitors [17,19].

In this work, we investigate the influence of the surface chemistry of $Ti_3C_2T_x$ on its electrochemical performance in the acidic electrolyte sulfuric acid, chosen due to its excellent electrical conductivity (0.26 S·cm^{-1} at 1 M). As-produced $Ti_3C_2T_x$ has a moderate SSA of 23 m^2·g^{-1} and is terminated with −F and −OH/═O functional groups, where the −F group may be a detriment to charge storage and F$^-$ is not known to participate in any pseudocapacitive energy storage processes. Therefore, our goal was to chemically modify $Ti_3C_2T_x$ using two

* Corresponding author at: Université Paul Sabatier, CIRIMAT UMR CNRS 5085, 118 route de Narbonne, 31062 Toulouse, France. Tel.: + 33 5 61 55 68 02.
E-mail address: simon@chimie.ups-tlse.fr (P. Simon).

different processes: 1) given the known intercalation of polar molecules and cations between $Ti_3C_2T_x$ layers [16,19], treatment in basic aqueous solutions should replace – F terminal groups with hydroxyl groups as Ti–F bonds become unstable at high pH [28]; 2) the intercalation of DMSO is known to lead to delamination of individual $Ti_3C_2T_x$ layers, giving an increase in an electrode's SSA up to ~100 $m^2 \cdot g^{-1}$ [17] and allowing for the water access and atmospheric oxidation of the $Ti_3C_2T_x$ surface. To monitor these processes, the structure and chemistry of the $Ti_3C_2T_x$ electrodes were analyzed by XRD and XPS.

2. Experimental

The multilayer $Ti_3C_2T_x$ was modified by chemical treatment in aqueous solutions with 1 molar salt concentration; 0.4 g of Ti_3C_2 was added to 50 mL of the salt solution, stirred for an hour; then the solution was decanted after powder sedimentation, this process was repeated 5 times. The SSA of MXene was not affected by the intercalation of these salts.

A scanning electron microscope (Zeiss, Supra 50VP, Oberkochen, Germany) was used to investigate the morphology of the samples. X-ray diffraction patterns were recorded with a powder diffractometer (Rigaku SmartLab) using Cu K_α radiation ($\lambda = 1.54$ Å) with 0.01° 2θ steps and 6 s dwelling time. An X-ray photoelectron spectrometer (VersaProbe 5000, Physical Electronics Inc., USA) employing a 100 μm monochromatic Al Kα X-ray beam to irradiate the surface of the samples was used to obtain XPS spectra. Emitted photoelectrons were collected using a 180° hemispherical electron energy analyzer. Samples were analyzed at a 45° takeoff angle between the sample surface and the path to the analyzer. High-resolution spectra were taken at a pass energy of 23.50 eV and with a step size of 0.05 eV. The peak fitting was carried out using CasaXPS Version 2.3.16 RP 1.6.

The electrochemical performance was tested using a VMP3 potentiostat (Biologic, S.A.) with a three-electrode Swagelok cell with Ag/AgCl as reference electrode and overcapacitive activated carbon as counter electrode. Multilayer Ti_3C_2 electrodes were mixed in ethanol with 5 wt.% polytetrafluoroethylene binder (60 wt.% in H_2O, Aldrich) and 5 wt.% carbon black (Alfa Aesar), then rolled and cut into 7 mm diameter disks with a thickness between 50 μm and 70 μm. The electrodes had an average mass loading of 2.6 mg and densities of 0.79 $g \cdot cm^{-3}$, 1.37 $g \cdot cm^{-3}$ and 1.51 $g \cdot cm^{-3}$ for $Ti_3C_2T_x$, KOH–Ti_3C_2 and KOAc–Ti_3C_2 electrodes, respectively. Delamination of $Ti_3C_2T_x$ was performed by DMSO intercalation, as described elsewhere [17].

The colloidal suspension was filtered using a cellulose-ester filter (Fisher Scientific) to obtain an 8 μm free-standing paper with a density of 1.62 $g \cdot cm^{-3}$, later cut into 25–35 mm^2 square electrodes.

3. Results and discussion

Fig. 1 shows a schematic view of these two chemical modification paths for $Ti_3C_2T_x$. The schematic's top right corner depicts treatment resulting in synthesis of delaminated layers of Ti_3C_2, denoted as d-Ti_3C_2. The bottom right corner schematic in Fig. 1 represents a K^+ ion chemically intercalated into $Ti_3C_2T_x$. Potassium hydroxide and potassium acetate were selected as the two salts to be intercalated into $Ti_3C_2T_x$, to probe the effect of the anion on the $Ti_3C_2T_x$ surface chemistry.

X-ray diffraction (XRD) patterns of $Ti_3C_2T_x$, KOH–Ti_3C_2, KOAc–Ti_3C_2 and d-Ti_3C_2 are shown in Fig. 2A. The intercalation of species between layers induces an increase in the c-lattice parameter (which defines distance between single Ti_3C_2 sheets), noticeable by the 2θ downshift of the (0002) peak position compared to $Ti_3C_2T_x$. The two chemicals (KOH and KOAc) share the same cation, thus the difference in their c-lattice parameter is related to other factors, such as pH. Yet, despite of acetate ion being larger than hydroxide ion, KOH–Ti_3C_2 has a larger c-lattice parameter than KOAc–Ti_3C_2, thus the difference cannot be directly correlated with the size of the anion. As discussed below, the KOH and KOAc treatments lead to two different surface chemistries, which may have an effect on the c-lattice parameter.

X-ray photoelectron spectroscopy (XPS) was used to characterize the surface chemistry of the samples. High-resolution XPS spectra of the samples ($Ti_3C_2T_x$, KOH–Ti_3C_2, KOAc–Ti_3C_2 and d-Ti_3C_2, shown in Fig. 2B–D) in the F 1s region indicated that the $Ti_3C_2T_x$ sample contained a large amount of F-terminated Ti (Fig. 2B). It was also noticed that AlF_3 salt residue from MAX phase etching was only present in the KOAc–Ti_3C_2 and $Ti_3C_2T_x$ samples. It was completely removed after KOH or DMSO treatment. The intensity of the Ti–F peaks decreases in the order d-Ti_3C_2, KOAc–Ti_3C_2, and KOH–Ti_3C_2, being the lowest for the latter one. The signal of the Ti–F component, which was initially at 684.4 eV, shifts toward a higher-binding energy as F is removed from Ti as fluoride salt.

Due to the 2D-nature of the $Ti_3C_2T_x$, oxidation does not proceed homogeneously and likely starts from the outer edges of the $Ti_3C_2T_x$ grains, giving oxides and mixed carboxides (TiC_xO_y) at the flake edges and on the outermost surface layer of the multilayer particle, while $Ti_3C_2T_x$ remains in the center of the grain. This inhomogeneity gives
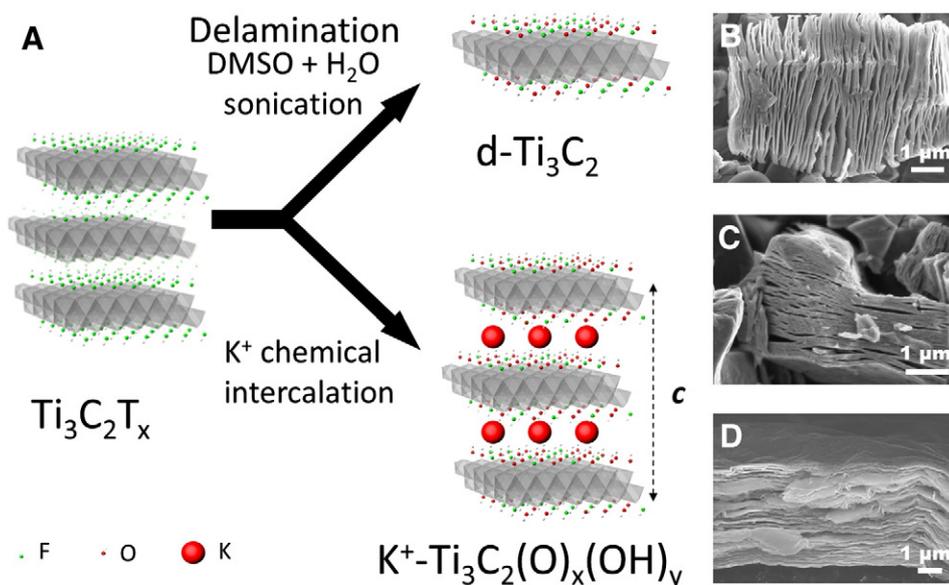

Fig. 1. (A) Schematic illustration of the modifications of $Ti_3C_2T_x$; delamination and intercalation of K^+. Scanning electron microscope images of (B) $Ti_3C_2T_x$, (C) KOH–Ti_3C_2 and (D) d-Ti_3C_2.
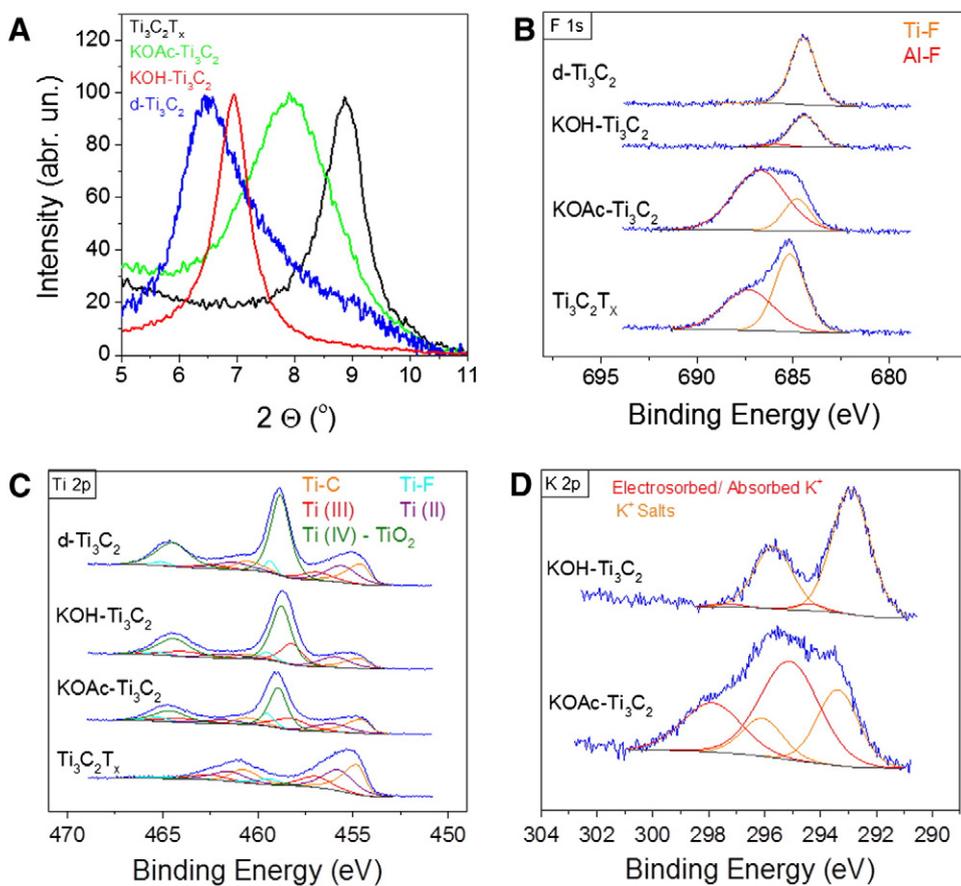
Fig. 2. Characterization data of Ti$_3$C$_2$-based materials after surface modification in various intercalation agents: (A) XRD in the (0002) peak region, and (B–D) high-resolution XPS spectra in the F 1s region, Ti 2p region and K 2p region, respectively.
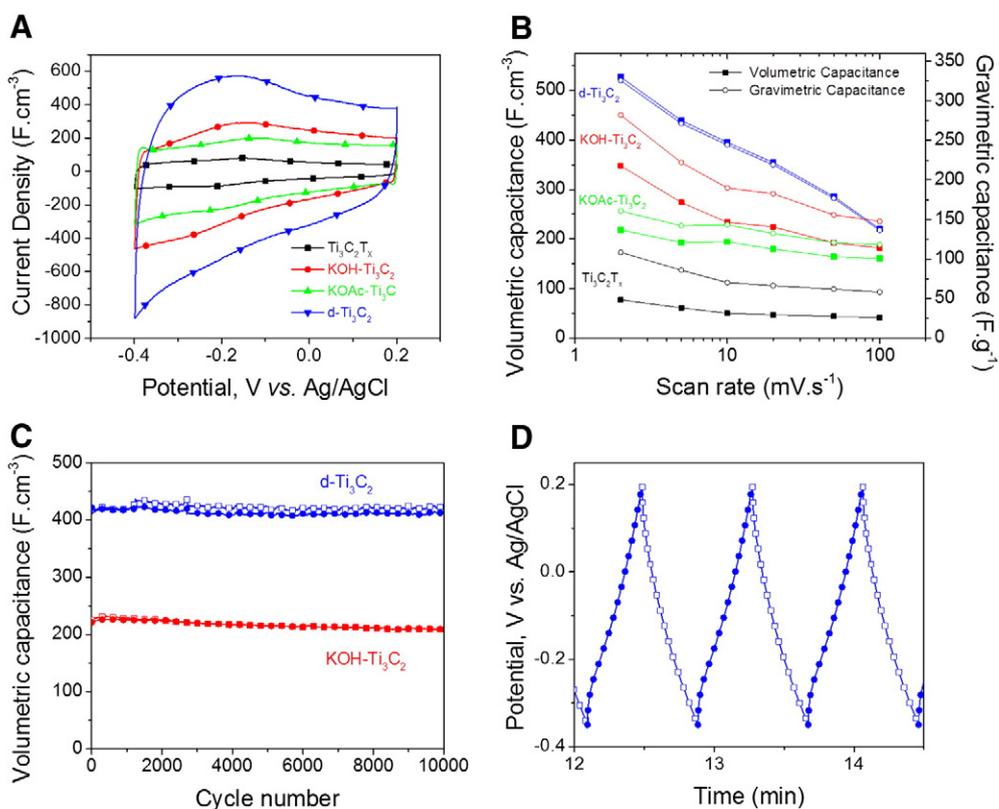

Fig. 3. Electrochemical performance of Ti$_3$C$_2$-based electrodes in 1 M H$_2$SO$_4$ (A) CV profiles at 10 mV·s^{-1} (B) Summary of rate performances. (C) Charge and discharge volumetric capacitance vs. cycle number of KOH–Ti$_3$C$_2$ and d-Ti$_3$C$_2$ electrodes from galvanostatic cycling at 5 A·g^{-1}. (D) Galvanostatic charge–discharge profile of d-Ti$_3$C$_2$.

rise to the broadened and convoluted spectra seen in the Ti 2p region (Fig. 2C). In this region, the Ti-carbide photoemission arises from Ti_3C_2, while the Ti (II) and Ti (III) components arise from these mixed oxides and carboxides, and the Ti (IV) component arises from TiO_2 present on the surface of the grains as oxidation goes to completion. These spectra also include a component for Ti–F that becomes less prominent and merges with that for Ti (IV), likely as a result of the formation of a small amount of the intermediate, fluorinated TiO_2, as hydroxyl groups replace the – F termination during the oxidation of the outer surface of Ti_3C_2. This region also indicates oxidation of the surface of the $Ti_3C_2T_x$ grains to Ti (IV) (TiO_2) for all modified $Ti_3C_2T_x$ samples. Accordingly, instead of F-termination, the KOH–Ti_3C_2, KOAc–Ti_3C_2 and d-Ti_3C_2 surfaces are terminated with oxygen-containing groups. High-resolution spectra of the samples in the K 1s region (Fig. 2D) reveal two components, the first is for K^+ that is strongly electrosorbed and the second component suggests that K^+ is present as salt, probably KF. The electrosorbed K^+ is much more prevalent in KOAc–Ti_3C_2 than in KOH–Ti_3C_2.

Fig. 3A shows the cyclic voltammograms (CVs) of all samples tested at 10 mV·s^{-1} sweep rate in aqueous 1 M H_2SO_4. Upon cycling, none of the materials presented a change in the c-lattice parameters as measured using XRD. A possible explanation is that the distance between two Ti_3C_2 layers is large enough that the intercalation of small H^+ has no effect on the c-lattice parameter. The best performances were achieved using d-Ti_3C_2 electrodes, with an outstanding volumetric capacitance of 520 F·cm^{-3} and a gravimetric capacitance of 325 F·g^{-1} at 2 mV·s^{-1} (Fig. 3B). We believe that the superior performances of d-Ti_3C_2 electrodes originate from several sources. First, it is a 6 times thinner electrode, leading to better charge transfer. It also has a higher specific surface area and is denser because of its morphology (aligned MXene flakes). Nonetheless, d-Ti_3C_2 has shown a stronger dependence of performance on the scan rate, which is assumed to be caused by the flakes aligning parallel to the current collector and increasing the transport path for ions as the film thickness increases.

The $Ti_3C_2T_x$, KOH–Ti_3C_2 and KOAc–Ti_3C_2 electrodes have the same SSA, therefore the difference in electrochemical performance can only be related to the difference in surface chemistry. The moderate capacitances for $Ti_3C_2T_x$ are consistent with the absence of redox activity of the F-termination. The KOAc–Ti_3C_2 and KOH–Ti_3C_2 electrodes exhibit similar behavior, with the latter having a higher gravimetric capacitance thanks to a lower content of F-groups (Fig. 2B). Their surfaces are terminated by oxygen-containing groups, including – OOH, =O and – OH, which are known to be responsible for pseudocapacitive behavior of carbon in acidic electrolytes. This hypothesis is consistent with the shape of the CVs presented in Fig. 3B, where the presence of a set of broad peaks at −0.2 and −0.1 V/Ref is observed. These peaks may originate from surface redox reactions of MXene leading to changes in the degree of oxidation of titanium in MXene, which is a transition metal capable of changing the oxidation degree between +3 and +4.

Fig. 3C shows the capacitance vs. cycle number dependencies obtained from galvanostatic charge–discharge curves shown in Fig. 3D. Stable capacitances of 415 F·cm^{-3} and 215 F·cm^{-3} were obtained at 5 A·g^{-1} for d-Ti_3C_2 and KOH–Ti_3C_2, respectively. After 10 000 cycles, no significant degradation was observed.

4. Conclusions

The effects of intercalation and delamination of the two-dimensional titanium carbide, $Ti_3C_2T_x$ (MXene) on its surface chemistry and electrochemical capacitance have been demonstrated. XPS analysis confirmed that terminal fluorine was successfully replaced with oxygen-containing functional groups after the chemical intercalation of potassium salts. This change in surface chemistry led to a 4-fold increase in the capacitance in sulfuric acid, demonstrating a pseudocapacitive contribution to the electrochemical behavior of MXene. Delamination of $Ti_3C_2T_x$ layers led to both an increase of the specific surface area of MXene films and the modification of the surface chemistry of d-$Ti_3C_2T_x$. These changes gave rise to an electrochemical capacitance of 520 F·cm^{-3} at 2 mV·s^{-1}, the highest volumetric capacitance reported for this material. Since Ti_3C_2 is a representative of a large family of two-dimensional transition metal carbides/nitrides, there is high probability that other MXenes can achieve even higher capacitance values, if their composition and surface chemistry are properly controlled.

Conflict of interest

There is no conflict of interest.

References

[1] P.G. Bruce, B. Scrosati, J.M. Tarascon, Nanomaterials for rechargeable lithium batteries, Angew. Chem. Int. Ed. 47 (2008) 2930–2946.
[2] J.R. Miller, P. Simon, Electrochemical capacitors for energy management, Science 321 (2008) 651–652.
[3] P. Simon, Y. Gogotsi, B. Dunn, Where do batteries end and supercapacitors begin? Science 343 (2014) 1210–1211.
[4] P. Simon, Y. Gogotsi, Capacitive energy storage in nanostructured carbon–electrolyte systems, Acc. Chem. Res. 46 (2013) 1094–1103.
[5] J.P. Zheng, P.J. Cygan, T.R. Jow, Hydrous ruthenium oxide as an electrode material for electrochemical capacitors, J. Electrochem. Soc. 142 (1995) 2699–2703.
[6] H.Y. Lee, J.B. Goodenough, Supercapacitor behavior with KCl electrolyte, J. Solid State Chem. 144 (1999) 220–223.
[7] V. Augustyn, P. Simon, B. Dunn, Pseudocapacitive oxide materials for high-rate electrochemical energy storage, Energy Environ. Sci. 7 (2014) 1597–1614.
[8] D. Rochefort, A.L. Pont, Pseudocapacitive behaviour of RuO_2 in a proton exchange ionic liquid, Electrochem. Commun. 8 (2006) 1539–1543.
[9] S. Chen, J.W. Zhu, X.D. Wu, Q.F. Han, X. Wang, Graphene oxide–MnO_2 nanocomposites for supercapacitors, ACS Nano 4 (2010) 2822–2830.
[10] K.W. Nam, C.W. Lee, X.Q. Yang, B.W. Cho, W.S. Yoon, K.B. Kim, Electrodeposited manganese oxides on three-dimensional carbon nanotube substrate: supercapacitive behaviour in aqueous and organic electrolytes, J. Power Sources 188 (2009) 323–331.
[11] Z.S. Wu, D.W. Wang, W. Ren, J. Zhao, G. Zhou, F. Li, H.M. Cheng, Anchoring hydrous RuO_2 on graphene sheets for high-performance electrochemical capacitors, Adv. Funct. Mater. 20 (2010) 3595–3602.
[12] A.L.M. Reddy, S. Ramaprabhu, Nanocrystalline metal oxides dispersed multiwalled carbon nanotubes as supercapacitor electrodes, J. Phys. Chem. C 111 (2007) 7727–7734.
[13] Y. Hou, Y.W. Cheng, T. Hobson, J. Liu, Design and synthesis of hierarchical MnO_2 nanospheres/carbon nanotubes/conducting polymer ternary composite for high performance electrochemical electrodes, Nano Lett. 10 (2010) 2727–2733.
[14] M.D. Stoller, S.J. Park, Y.W. Zhu, J.H. An, R.S. Ruoff, Graphene-based ultracapacitors, Nano Lett. 8 (2008) 3498–3502.
[15] A. Janes, H. Kurig, E. Lust, Characterisation of activated nanoporous carbon for supercapacitor electrode materials, Carbon 45 (2007) 1226–1233.
[16] M. Naguib, O. Mashtalir, J. Carle, V. Presser, J. Lu, L. Hultman, Y. Gogotsi, M.W. Barsoum, Two-dimensional transition metal carbides, ACS Nano 6 (2012) 1322–1331.
[17] O. Mashtalir, M. Naguib, V.N. Mochalin, Y. Dall'Agnese, M. Heon, M.W. Barsoum, Y. Gogotsi, Intercalation and delamination of layered carbides and carbonitrides, Nat. Commun. 4 (2013).
[18] D. Sun, M. Wang, Z. Li, G. Fan, L.-Z. Fan, A. Zhou, Two-dimensional Ti_3C_2 as anode material for Li-ion batteries, Electrochem. Commun. 47 (2014) 80–83.
[19] M.R. Lukatskaya, O. Mashtalir, C.E. Ren, Y. Dall'Agnese, P. Rozier, P.L. Taberna, M. Naguib, P. Simon, M.W. Barsoum, Y. Gogotsi, Cation intercalation and high volumetric capacitance of two-dimensional titanium carbide, Science 341 (2013) 1502–1505.
[20] M.D. Levi, M.R. Lukatskaya, S. Sigalov, M. Beidaghi, N. Shpigel, L. Daikhin, D. Aurbach, M.W. Barsoum, Y. Gogotsi, Solving the capacitive paradox of 2D MXene using electrochemical quartz-crystal admittance and in situ electronic conductance measurements, Adv. Energy Mater. (2014), http://dx.doi.org/10.1002/aenm.201400815.

[21] M. Naguib, J. Come, B. Dyatkin, V. Presser, P.-L. Taberna, P. Simon, M.W. Barsoum, Y. Gogotsi, MXene: a promising transition metal carbide anode for lithium-ion batteries, Electrochem. Commun. 16 (2012) 61–64.

[22] J. Come, M. Naguib, P. Rozier, M.W. Barsoum, Y. Gogotsi, P.L. Taberna, M. Morcrette, P. Simon, A non-aqueous asymmetric cell with a Ti_2C-based two-dimensional negative electrode, J. Electrochem. Soc. 159 (2012) A1368–A1373.

[23] Q. Tang, Z. Zhou, P.W. Shen, Are MXenes promising anode materials for li ion batteries? Computational studies on electronic properties and Li storage capability of Ti_3C_2 and $Ti_3C_2X_2$ (X=F, OH) Monolayer, J. Am. Chem. Soc. 134 (2012) 16909–16916.

[24] Q.K. Hu, D.D. Sun, Q.H. Wu, H.Y. Wang, L.B. Wang, B.Z. Liu, A.G. Zhou, J.L. He, MXene: a new family of promising hydrogen storage medium, J. Phys. Chem. A 117 (2013) 14253–14260.

[25] M. Khazaei, M. Arai, T. Sasaki, C.Y. Chung, N.S. Venkataramanan, M. Estili, Y. Sakka, Y. Kawazoe, Novel electronic and magnetic properties of two-dimensional transition metal carbides and nitrides, Adv. Funct. Mater. 23 (2013) 2185–2192.

[26] M. Naguib, M. Kurtoglu, V. Presser, J. Lu, J.J. Niu, M. Heon, L. Hultman, Y. Gogotsi, M. W. Barsoum, Two-dimensional nanocrystals produced by exfoliation of Ti_3AlC_2, Adv. Mater. 23 (2011) 4248–4253.

[27] M.W. Barsoum, The $M_{(N+1)}AX_{(N)}$ phases: a new class of solids; thermodynamically stable nanolaminates, Prog. Solid State Chem. 28 (2000) 201–281.

[28] Y. Xie, M. Naguib, V.N. Mochalin, M.W. Barsoum, Y. Gogotsi, X. Yu, K.-W. Nam, X.-Q. Yang, A.I. Kolesnikov, P.R.C. Kent, Role of surface structure on Li-ion energy storage capacity of two-dimensional transition-metal carbides, J. Am. Chem. Soc. 136 (2014) 6385–6394.